European Polymer Journal 152 (2021) 110467

Contents lists available at ScienceDirect

European Polymer Journal

journal homepage: www.elsevier.com/locate/europolj

Luminescent gold nanocluster-decorated polymeric hybrid particles for laser guided therapy

Erik R. Hebels [a], Marzieh Najafi [a], Joep van den Dikkenberg [a], Nataliia Beztsinna [a], Sanne van de Looij [a], Danny Wilbie [a], Johannes Meeldijk [b], Mathew Hembury [a], Tina Vermonden [a,*]

[a] Department of Pharmaceutics, Utrecht Institute for Pharmaceutical Sciences (UIPS), Science for Life, Utrecht University, P.O. Box 80082, 3508 TB Utrecht, the Netherlands

[b] Electron Microscopy Group, Utrecht University, Padualaan 8, 3584 CH Utrecht, the Netherlands

ARTICLE INFO

Keywords:
Near infra-red
Reversible Addition-Fragmentation Chain Transfer (RAFT) polymerization
Doxorubicin
Polymeric micelles
Laser guided therapy

ABSTRACT

Gold nanoclusters or ultrasmall gold atom clusters (AuNCs, <2 nm in diameter) exhibit emergent photonic properties in the near-infrared (NIR) spectrum due to the quantization of their conduction band. This gives rise to attractive NIR luminescent properties that offer great promises for imaging and diagnostic purposes in biomedical applications. AuNCs also absorb NIR light in the biological window inducing photothermal events that can facilitate localized drug release and synergistic thermal therapy. Here, we designed a micellar system based on poly(ethylene glycol) (PEG) and thermosensitive poly(*N*-isopropylacrylamide) (PNIPAM) copolymerized with functional monomers to allow for micellar core-crosslinking via oxo-ester mediated native chemical ligation (OMNCL). These micelles are decorated with AuNCs (<2 nm) and covalently bound thiolated doxorubicin, which allow for both precise intracellular imaging as well as light-induced cell killing. The polymer bound AuNCs exhibit a NIR luminescent emission maximum at ~ 720 nm with a quantum yield of ~ 3%. Internalization studies of the micellar system on MDA-MB-231 cancer cells showed that doxorubicin remains bound within the micelles in the cytosolic region after 24 h incubation. Upon NIR light irradiation at 650 nm, highly localized cell death is observed, which is limited only to the irradiated area. This innovative hybrid material design of the the AuNC-decorated micelles enables an efficient combination of live imaging and precisely controlled therapy.

1. Introduction

Gold particles in the nanometer size range have received increasing attention in the past decade for biomedical applications due to their interesting physical properties and physiological compatibility.[1,2] In the sub-100 nm size range, gold nanoparticles exhibit plasmonic properties that allow transduction of optical and near infra-red (NIR) light into heat and thereby present opportunities for laser guided drug delivery.[3] Gold nanoparticles have been extensively investigated as drug delivery tools themselves, but they have also been incorporated into various other drug delivery systems such as liposomes to aid cargo protection.[4,5] By employing temperature-labile interactions to encapsulate drug molecules into such a gold nanoparticle containing system, the production of heat can serve as the trigger to release drug molecules in a localized fashion upon light irradiation. Additionally, the localized heating effects produced can contribute to synergistic treatment actions, particularly for the cytotoxic action of chemotherapeutics (*e.g.* Doxorubicin and Cisplatin).[6-8] Furthermore, gold nanoparticles approaching the low nanometer size range (<2 nm, ~200–300 atoms) start exhibiting molecule like properties. In contrast to larger plasmonic gold nanoparticles (>2 nm), these ultrasmall gold nanoparticles or gold nanoclusters (AuNCs) possess discrete electronic energy levels allowing for one-electron HOMO-LUMO transitions as opposed to collective-electron plasmon excitation.[9] This additional property allows for luminescent features that can be employed for diagnostic applications.[2]

Light in the NIR region (650–900 nm) is particularly interesting as a trigger for therapeutic and diagnostic purposes as it is well tolerated by healthy cells as compared to other forms of light currently applied in oncology, such as X-rays. By being within the so-called biological

* Corresponding author.
E-mail address: T.Vermonden@uu.nl (T. Vermonden).

https://doi.org/10.1016/j.eurpolymj.2021.110467
Received 25 October 2020; Received in revised form 26 February 2021; Accepted 6 April 2021
Available online 20 April 2021

absorption window, NIR light still retains high levels of tissue penetration when compared to wavelengths in the optical spectrum.[10,11] For this reason, recent interest in developing systems utilizing NIR light to induce photothermal effects, two-photon excitations and upconversions for the triggered release of drug compounds from nanocarrier systems for cancer therapy has increased.[12]

With regards to photothermal based cancer therapy, the ideal nanocarrier should possess strong light absorption, small particle size for deep tumor penetration, controlled surface chemistry allowing systemic administration and long circulation times, low inherent toxicity as well as biodegradability. For this purpose, the use of polymeric micelles as nanocarriers is of particular interest and such systems have previously been described combined with gold nanorods for triggered release of doxorubicin (DOX)[13] and photothermal cell killing by delivery of IR-780.[14] However, gold nanoparticle (>2 nm) and nanocluster (<2 nm) containing micellar systems described to date typically feature non-core-crosslinked polymeric micelles, which could negatively affect formulation stability *in vivo*. Furthermore, drug loading in these hybrid systems is typically based on hydrophobic interactions instead of covalent bonding which could lead to premature drug release *in vivo*.[15-17] Finally, AuNCs (<2 nm) have primarily only been explored for use as diagnostic tools [18] and for the tracking of drug loaded nanocarriers.[19-21] The few examples existing for AuNC incorporated NIR triggered cytotoxicity systems are aimed at photodynamic therapy or release of non-covalently entrapped chemotherapeutic agents.[22-24]

Previously, we showed that AuNCs with imaging capabilities could be formed onto thermosensitive amphiphilic polymers formed by reversible addition − fragmentation chain transfer (RAFT) polymerization by use of free thiol endcaps obtained after aminolysis of the chain transfer agent.[2] Here, we re-designed this approach to a core-crosslinked micellar system based on thermosensitive poly(ethylene glycol)$_{5000}$-poly(*N*-isopropylacrylamide-co-*N*-hydroxypropyl methacrylamide-cysteine) (**PNC**) and a complementary polymer, poly (ethylene glycol)$_{5000}$-poly(*N*-isopropylacrylamide-*co*-acrylic acid *N*-hydroxysuccinimide) (**PNA**). The thermosensitive blocks of *N*-isopropyl acrylamide (NIPAM) allow these polymers to self-assemble into micelles upon increasing temperature.[25] Upon micelle formation, physiologically irreversible amide bonds are formed *via* oxo-ester mediated native chemical ligation (OMNCL), resulting in covalently core crosslinked micelles with free thiols to allow formation of AuNCs. [26] The aim of this study was to investigate whether AuNCs together with thiol-derivatized doxorubicin (DOX) could be incorporated stably in these micelles via the excess free thiols in the core of the micelles and to investigate the potential of this hybrid drug delivery system for use against resilient tumor cells. To this purpose, the system was evaluated for laser triggered drug release and cancer cell killing showing its potential as highly localized photothermal anti-cancer treatment.

2. Materials and methods

All materials were obtained from Sigma Aldrich (Zwijndrecht, The Netherlands) unless indicated otherwise. Boc-Cysteine(Acm)-*N*-hydroxypropylacrylamide (Boc-Cys(Acm)-HPMA) was synthesized according to a previously described procedure.[27] Dimethylformamide (DMF), dichloromethane (DCM), trifluoroacetic acid (TFA) and diethyl ether were obtained from Biosolve (Valkenswaard, The Netherlands). Phosphate buffered saline (PBS buffer) pH 7.4 (8.2 g/L NaCl, 3.1 g/L $Na_2HPO_4{\cdot}12H_2O$, 0.3 g/L $NaH_2PO_4{\cdot}2H_2O$) was purchased from B. Braun (Melsungen, Germany). Dulbecco's Modified Eagle Medium (DMEM) high glucose content and fetal bovine serum (FBS) were purchased from Sigma-Aldrich (Zwijndrecht, The Netherlands). Phenol red free Opti-MEM medium was purchased from Thermo Fisher Scientific (Bleiswijk, The Netherlands).

2.1. Synthesis

2.1.1. Reversible addition−fragmentation chain transfer (RAFT) polymerization of poly(ethylene glycol)$_{5000}$-poly(N-isopropylacrylamide-co-N-hydroxypropyl methacrylamide-cysteine) (PNC)

Poly(ethylene glycol) methyl ether 2-(dodecylthiocarbonothioylthio)-2-methylpropionate (PEG$_{5000}$-CTA, 1 g, 0.19 mmol), *N*-isopropylacrylamide (NIPAM, 2 g, 18 mmol), 2,2′-azobis(2-methylpropionitrile) (AIBN, 6 mg, 0.04 mmol) as initiator ([CTA]:[AIBN] = 5:1), Boc-Cys(Acm)-HPMA (0.54 g, 1.3 mmol) and dry DMF (to acquire a monomer concentration of 300 mg/mL) were added into a Schlenk flask and the mixture was degassed by 4 freeze-vacuum-thaw cycles, backfilled with N_2 gas and placed in an oil bath at 70 °C. After 45 h, the polymer was precipitated in cold diethyl ether, centrifuged, washed with cold diethyl ether and dried under N_2 flow. ^{1}H NMR and GPC were used to characterize the protected polymer.

The Boc protecting groups were removed by dissolving the obtained diblock polymer in DCM/TFA (1:1 v/v, 100 mL) and stirring for 2 h at room temperature. The polymer was then precipitated in diethyl ether and a solid was obtained by vacuum filtration. The Acm protecting groups were removed by dissolving the polymer in MeOH/H2O (1:1 v/v, 100 mL) under a N_2 atmosphere followed by addition of HCl (1 M, 1 mL) and iodine in MeOH (0.2 M, 16 mL). This brown mixture was stirred for 1 h at RT after which the excess iodine was quenched using some drops of 1 M ascorbic acid solution and the solution was neutralized by addition of Na_2CO_3. TCEP (500 mg, 2 mmol) was added to the solution to reduce the formed disulfide bridges and this mixture was stirred for 16 h. Dialysis was performed using 12–14 kDa cutoff membranes at room temperature for 3 days. The final deprotected polymer was obtained after lyophilization and characterized by ^{1}H NMR and GPC. Free primary amines (from HPMA-cysteine monomers) were detected by TNBSA assay.[28]

2.1.2. RAFT polymerization of poly(ethylene glycol)$_{5000}$-poly(N-isopropylacrylamide-co-acrylic acid N-hydroxysuccinimide) (PNA)

Poly(ethylene glycol) methyl ether 2-(dodecylthiocarbonothioylthio)-2-methylpropionate (PEG$_{5000}$-CTA, 0.5 g, 0.09 mmol), *N*-isopropylacrylamide (NIPAM, 1 g, 9 mmol), 2,2′-azobis(2-methylpropionitrile) (AIBN, 3 mg, 0.02 mmol) as initiator ([CTA]:[AIBN] = 5:1), Acrylic acid *N*-hydroxysuccinimide (NAS, 0.1 g, 0.6 mmol) and dry DMF (to acquire a monomer concentration of 300 mg/mL) were added into a Schlenk flask and the mixture was degassed by 4 freeze-vacuum-thaw cycles, backfilled with N_2 gas and placed in an oil bath at 70 °C. After 45 h, the polymer was precipitated in cold diethyl ether, centrifuged, washed with cold diethyl ether and dried under N_2 flow. Characterization was done by ^{1}H NMR and GPC.

2.1.3. Core-crosslinked micelle synthesis

PNC and PNA polymers were dissolved seperately in PBS in an ice bath with a polymer concentration of 30 mg/mL. After 2 h of dissolution, the polymer solutions were mixed at a 2:1 PNC to PNA ratio and pipetted into PBS at 55 ℃ in an oil bath reaching a final polymer concentration of 5 mg/mL and the reaction was left to proceed for 2 h. For cell experiments, particle formulations were purified with two runs through PD10 columns employing milliQ water as eluent and filtered through a 0.45 μm syringe filter.

2.1.4. Gold nanocluster formation

Typically, AuNCs were formed by addition of $HAuCl_4{\cdot}2H_2O$ to the core-crosslinked micelle solution in PBS at a molar ratio of 3:1 of thiol (based on monomer determination by ^{1}H NMR) to Au unless mentioned otherwise. After 1 h of stirring, 3 eq. relative to Au of aqueous $NaBH_4$ was added to reduce nucleated gold clusters to Au(0) and the solution was left to stir for 16 h.

2.1.5. DOX thiol modification (DOX-SH)

Thiol moieties were introduced onto doxorubicin using 2-iminothiolane (Traut's reagent).[29] DOX.HCl (56 mg, 97 μmol) was weighed into a small reaction flask and dissolved in 1 mL DMF. The 2-iminothiolane (19 mg, 140 μmol) was dissolved in 2 mL DMF and triethylamine (TEA) (40 μL, 292 μmol) was added before transferring this solution to the DOX.HCl solution. The reaction mixture was stirred for 16 h at RT after which the product was precipitated in cold diethyl ether, centrifuged, washed with diethyl ether and a solid red crystalline powder was obtained. Characterization was done using ^{1}H NMR, ESI-MS and LC-MS.

DOX-SH was incorporated into the core-crosslinked micelles during the gold nanocluster formation, employing 2 mol eq. relative to the PNC polymer.

2.2. Polymer and particle characterization

2.2.1. Magnetic resonance (NMR) spectroscopy

^{1}H NMR (400 MHz) spectra were measured on an Agilent 400-MR NMR spectrometer (Agilent Technologies, Santa Clara, USA). The residual solvent peak of $CDCl_3$ (δ = 7.26 ppm) was used to calibrate chemical shifts.

2.2.2. Gel permeation chromatography (GPC)

GPC was performed using a PLgel 5 μm mixed-D column (Polymer Laboratories) and employing a refractive index detector (RID). DMF containing 10 mM LiCl was used as eluent. The elution rate was set to 1 mL min^{-1} and the column temperature was set to 65 °C. The typical sample concentration employed was 10 mg/mL. As calibration standards, PEG polymers of narrow and defined molecular weights were used.

2.2.3. Cloud point measurement

The cloud points of the PNIPAM containing polymers in PBS were determined by measurement of light scattering at a 90° angle upon the onset of opalescence. Scattered light intensity was measured using a Jasco FP-8300 spectrophotometer employing an excitation and emission wavelength of 550 nm with 1 nm slit width and a response time of 1 s. Temperature was ramped from 10 °C to 60 °C at 1 °C per minute.

2.2.4. Dynamic light scattering (DLS)

Particle size was investigated using DLS on a Malvern CGS-3 goniometer coupled to an ALV/LSE-5003 autocorrelator, with a temperature controlled sample holder and a He-Ne laser (25 mW, 633 nm). Measurements were done at 90° scattering angle at varying temperatures. Solvent viscosity was adjusted by the software and both z-average radius and polydispersity were calculated by the ALV and DTS software.

2.2.5. Photoluminescent profiling

A Jasco FP-8300 spectrophotometer was used to measure photoluminescence arising from the PNC bound AuNCs in 10 mm quartz cuvettes. A response time of 1 s, 5 nm slit width and resolution of 0.5 nm was employed. Emission spectra were recorded from 560 to 900 nm using an excitation wavelength of 550 nm and for temperature profiling, the temperature was ramped from 10 °C to 60 °C at 1 °C per minute.

2.2.6. Electron microscopy

Transmission Electron Microscopy (TEM) was employed to characterize the morphology of the AuNC containing micelles. Brightfield TEM and High Angle Annular Dark Field Scanning TEM (HAADF-STEM) images were obtained with a Tecnai20F (Thermo Fisher Scientific) microscope equipped with a model 694 Gatan CCD camera and an Energy-Dispersive X-ray Spectroscopy (EDS) detector (EDAX), employing an accelerating voltage of 200 kV. Samples were diluted in Milli-Q water (1 mg/mL) and left at the desired temperature (10 or 45 °C) for 30 min before being drop-deposited on 200 mesh carbon coated copper TEM grids (Agar Scientific) prior to analysis. Due to rapidly occurring sample damage, bright field TEM and HAADF-STEM images were not acquired on the same specimen locations. Images were scaled and processed using ImageJ.

2.2.7. UV–Vis spectroscopy

DOX-SH contained within the micelle formulations was quantified using 10 mm path-length disposable polystyrene cuvettes in a Shimadzu UV 2450 spectrophotometer at 500 nm. DOX.HCl was used as a reference standard (see SI Fig. 1) with calibrations ranging from 70 to 170 μM in milliQ and DOX-SH concentration within the micelle formulation determined after subtracting the absorbance of non-DOX-SH containing gold nanocluster micelles at the same particle concentration (2.5 mg/mL total polymer content).

Absorbance spectra measurements were recorded with a 0.5 nm resolution. For quantum yield determination, spectra were measured from 300 to 900 nm in 10 mm quartz cuvettes at 25 °C.

2.2.8. Quantum yield

Quantum Yields (QYs) of PNC bound AuNCs were measured using Qdot 800 Carbonyl Quantum Dots (Invitrogen; QY = 0.62) as a reference in milliQ water. Appropriate sample dilutions were made to minimize luminescence quenching due to internal reabsorption, keeping the extinction coefficient E below 0.2 absorbance at the excitation wavelength (550 nm). QYs were calculated according to the following equation;

$$QY = QY_{ref}\frac{In^2(1-10^{-E})^{ref}}{I_{ref}n_{ref}^2 1-10^{-E}}$$

where I is the integrated luminescence intensity (600–900 nm), n is the refractive index and *ref* denotes the Qdot 800 reference sample. [30]

2.2.9. Size exclusion chromatography

In order to analyze free drug and bound drug fractions, a desalting column from GE Healthcare was used (HiTrap 5 mL Sephadex G-25). The column was equilibrated using milliQ water or buffer (PBS pH 7.2 or ammonium acetate 10 mM, pH = 5) at a flow rate of 1 mL/min for 30 min and the samples were injected with a typical volume of 50 μL. Chromatograms were recorded with UV/Vis detection at wavelengths of 254 nm and 500 nm.

2.3. Cytotoxicity and Internalization studies

2.3.1. Cell culture

MDA-MB-231 cells were obtained from American Type Culture Collection (ATCC HTB-26), cultured and maintained at 37 °C in an incubator regulated with 5% CO_2, 95% air and saturated humidity. Roswell Park Memorial Institute (RPMI) 1640 medium supplemented with 10% Fetal Bovine Serum (FBS) was employed as the cell culture medium, no antibiotics were added. Cells were passaged upon reaching 80% confluency every 2–4 days using trypsin ethylenediaminetetraacetic acid (trypsin-EDTA).

2.3.2. DOX and DOX-SH IC_{50} measurements

MDA-MB-231 cells were plated onto black polystyrene (with microclear bottom) 96 well plates (Greiner #655090) at a density of 1×10^4 cells per well and incubated for 24 h. Free and micelle bound drugs were diluted to the appropriate concentrations with RPMI 10% FBS medium and 100 μL of each dilution added to the well plate after aspiration followed by another 100 μL of medium in triplicate. After incubation for either 24 h or 48 h, the medium was aspirated and 100 μL of alamarBlue stain diluted in medium was added (50 μM resazurin). After 2–3 h of incubation, fluorescence was recorded using a Mithras plate reader at 600 nm (λ_{ex} = 530 nm). Data were background subtracted and normalized by the fluorescence intensity recorded of untreated cells of the same well plate. The IC_{50} is defined as the drug concentration at 50%

cell viability.

2.3.3. Laser confocal scanning microscopy

MDA-MB-231 cells were plated onto 6-chamber Ibidi slides (Ibidi, Germany) with a cell density of 4×10^4 cells per chamber and incubated for 24 h. Free and micelle bound drugs were diluted to the appropriate concentrations with RPMI 10% FBS medium and 120 μL of each dilution added to the well plate after aspiration followed by another 30 μL of medium in triplicate. After 24 h of incubation time, medium was removed, the cells were washed 3 times with PBS and fixed with 4% (v/v) paraformaldehyde (PFA) in PBS. Before fixation, Hoechst 33342 stain (10 nM, 10 min at 37 °C) was used to stain the cell nuclei and Oregon Green labeled Wheat Germ Agglutinin (WGA) (5 ug/mL, 15 min at 37 °C) to stain cell membranes (Thermo Fisher Scientific, Naarden, The Netherlands). The slides were visualized using a confocal microscope (Leica TCS SP8 X MP), and the images were processed with LAS X (Leica Microsystems) and ImageJ.

2.3.4. Laser cytotoxicity and Life/Dead staining epifluorescence microscopy

MDA-MB-231 cells were plated onto 24 well plates (Greiner Cellstar) with a cell density of 4×10^4 cells per chamber and incubated for 24 h using Dulbecco's Modified Eagle Medium (DMEM). Drug formulations were added to a particle concentration of 1 mg/mL. After 24 h of incubation time, the medium was replaced with 150 μL phenol red free OptiMEM medium and the cells irradiated 60 min with a 650 nm laser at 300 mW. Cells were stained 24 h after laser irradiation with Calcein-AM/Propidium Iodide Life/Dead stain and imaged using a Keyence BZ-9000E epifluorescence microscope. BZ-II analyzer software was employed for imaging with GFP, DAPI and TexasRED filters and stitching.

3. Results and discussion

Reversible Addition − Fragmentation Chain Transfer (RAFT) polymerization was employed using a commercially available poly(ethylene glycol) (PEG) chain transfer agent targeting a conversion of approximatively 80% in order to obtain low polydispersity. The PNC polymer was synthesized to obtain a diblock polymer with a hydrophilic part of PEG_{5000} and a thermosensitive hydrophobic part of poly(*N*-isopropylacrylamide) (PNIPAM) that also contains cysteine residues from the copolymerized *N*-hydroxypropyl methacrylamide-cysteine) (HPMA-Cys) (Fig. 1A). A complementary polymer containing copolymerized acrylic acid *N*-hydroxysuccinimide (NAS) instead of HPMA-Cys was also synthesized to enable core-crosslinking of micelles formed with both PNC and PNA via oxo-ester mediated native chemical ligation (OMNCL). [26] Successful polymerization was confirmed by ^{1}H NMR (SI figs. 2–4) and gel permeation chromatography (GPC) of the PNA polymers and protected PNC polymers. The polymers were found to have a number-average molecular weight of 15.3 and 15.9 kDa, respectively (~85% conversion). Dispersity was found to be 1.5 and 1.4 for protected PNC and PNA, respectively. Furthermore, the cloud points for PNC and PNA polymers were 33 °C and 29 °C respectively, which is in line with previous results of polymers obtained by atom transfer radical polymerization (Fig. 1B). [31] RAFT polymerization was chosen here to fall in line with our previous study on AuNC incorporation into PEG_{5000}-*b*-PNIPAM-SH polymers. [2]

The presence of free thiol moieties in the deprotected PNC polymer was confirmed by Ellmann's assay, [32] though colorimetric quantification resulted in much lower values (2.0 equivalents per chain) than expected based on the amount of functional monomers detected by ^{1}H NMR of the protected polymer (6.0 equivalents per chain). Likely, disulfide formation and potentially steric hindrance within the micellar core prevented reaction with the Ellman's reagent. Instead, the amine groups of the cysteine residues were quantified using a trinitrobenzenesulfonic acid (TNBSA) assay following a previously published procedure, [32] which resulted in 5.7 amines per polymer chain corresponding to the ^{1}H NMR results.

AuNCs (<2 nm) were formed onto the PNC polymer using different weight ratios of gold(III) chloride trihydrate ($HAuCl_4 \cdot 3H_2O$). Different concentrations of gold salt solution were added to an excess of thiolated PNC polymers to form gold(I)-thiol complexes before the final reduction to gold(0) using sodium borohydride ($NaBH_4$) to investigate whether sufficient thiols are present for successful AuNC (<2 nm) formation. Their photoluminescent profiles (Fig. 1C) show a proportional increase in photoluminescent intensity with increasing gold content (having a peak emission wavelength of ~ 720 nm). [9,33] The absence of plasmonic peaks in the absorbance spectra indicates that no large gold nanoparticles have been formed (SI Fig. 5). Furthermore, the measured quantum yields were 3.0%, 3.0% and 2.5% for the 9:1, 4.5:1 and 3:1 (mol:mol, -SH:Au) ratios respectively. These quantum yields are comparable to polymer-gold nanocluster hybrids previously developed within our group (3.6%) [2] and significantly higher when compared to other gold nanocluster based systems described in the literature (<1%), indicating sufficient thiols are present for the gold quantities employed. [34,35]

The formation of core-crosslinked gold nanocluster micelles formed from PNC and PNA polymers using a heat shock procedure was investigated using two approaches: OMNCL-crosslinking before or after nanocluster formation (SI scheme 1). Both approaches resulted in AuNC containing micelles with sizes of around 60 nm diameter at room temperature. However, DLS measurements after addition of excess TCEP showed that stable micelles could only be achieved by first forming core-crosslinked micelles and subsequent formation of AuNCs. The inefficient core-crosslinking in the second method could be due to unavailable thiol

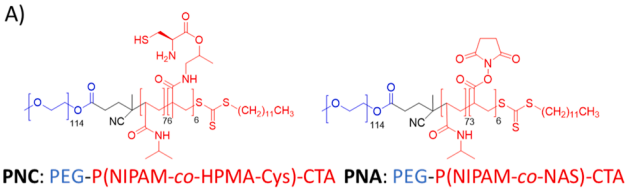

B)

	eq. NIPAM		eq. (HPMA-Cys or NAS)		M_n (kDa)[a]	M_n (kDa)[b]	PDI[b]	Cloud Point (°C)
	Feed	Obtained[a]	Feed	Obtained[a]				
PNC	97	76	7	6	15.9	16.0	1.5	33
PNA	97	73	7	6	15.3	15.0	1.4	29

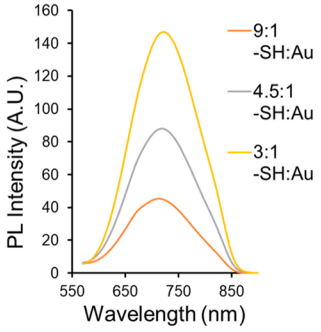

Fig. 1. A) Structures of PNC and PNA polymers. B) Table summarizing the physical and chemical properties of protected PNC and PNA polymers and C) photoluminescence (PL) spectra of PNC capped AuNCs ($\lambda_{ex} = 550$ nm) formed with 9:1 (orange), 4.5:1 (grey) and 3:1 (yellow) (mol:mol) of thiol to gold ratio. [a] Determined by ^{1}H NMR [b] Determined by GPC.

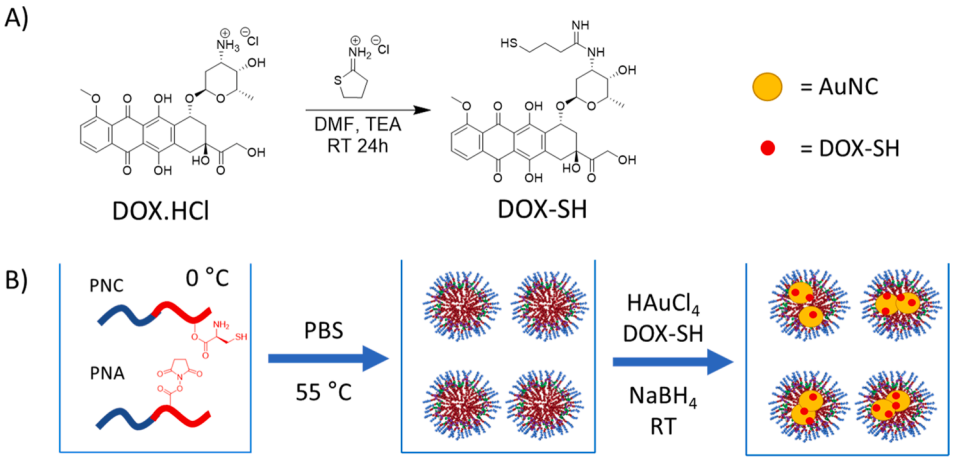

Scheme 1. Schematic representation of the modification of doxorubicin (A) and formation of core-crosslinked micelles (B) with simultaneous incorporation of DOX-SH and gold nanocluster formation into the pre-crosslinked PNC-PNA micelles.

moieties after nanocluster formation, which are required for the native chemical ligation reaction between PNC and PNA and potentially steric hindrance caused by the presence of AuNCs. It is therefore necessary to crosslink the polymers before the introduction of AuNCs. Hence, only results regarding this pre-crosslinking approach will further be discussed (Scheme 1B).

The temperature dependent photoluminescent profile of the gold nanocluster containing micelles was investigated. The photoluminescence profile of gold nanocluster containing micelles formed by the pre-crosslinking approach showed a spiked increase in intensity with increasing temperature (Fig. 2). This behavior is explained by the shrinkage of the micelles and consequent change in environment (SI table 1) bringing the AuNCs into closer proximity, which is consistent with the gold-polymer hybrids developed previously.[2] The highest intensity is found at a temperature of 37 °C, followed by a decrease in photoluminescent intensity due to thermal quenching effects, common to fluorophore behaviour.[36] Summarizing, the fluorescent properties of the AuNCs are retained with the pre-crosslinking approach and signal intensity is enhanced at a physiological temperature of 37 °C.

For the covalent incorporation of doxorubicin into the micelle formulation, doxorubicin was modified with 2-iminothiolane (Traut's reagent) to contain thiol functionalities (SI figs. 6&7). This allows for covalent attachment to the AuNCs or the polymer (scheme 1) to have the closest possible proximity towards the heat source and, therefore, the highest probability of subsequent release upon irradiation.[37] Furthermore, modification with 2-iminothiolane preserves the positive charge in the amino sugar moiety with a secondary amine. Although, recently it has been shown that free NH_2 groups are not essential for the cytostatic activity of anthracyclines.[38] Indeed, the IC_{50} of free DOX-SH and DOX.HCl on MDA-MB-231 cells after 48 h of drug incubation was found to be 12 μM and 1 μM respectively, showing a slight decrease in cytostatic activity of DOX after modification with 2-iminothiolane (SI fig. 9A). Successful DOX-SH encapsulation within the gold micelle system was shown by use of size exclusion (SI fig. 10). Upon addition of TCEP, DOX-SH is released confirming a thiol-based nature of encapsulation, which can be attributed to gold-thiol, thiol-thiol bonds or a mixture of both types of bonds. Micelles and free doxorubicin were separated with a HiTrap desalting column and a significant difference in retention time of both fractions was found (micelle bound fractions (Mr > 5000 Da) with an R_t of 2 min and free DOX-SH starting at an R_t of 10 min). This separation enabled the quantification of the DOX-SH content within the micelles by UV–Vis spectroscopy, which was found to be 105 μM for a 2.5 mg/mL (2.8% w/w loading) total polymer concentration micelle solution.

The presence of the AuNCs within the micelles was investigated by transmission electron microscopy (TEM). Fig. 3 shows the images obtained for AuNC micelles loaded with DOX-SH. In the bright field TEM, the observed dark clusters are closer together with increasing temperature, confirming the expected change in nanocluster proximity (Fig. 3A). The order of magnitude of the AuNC containing micelle area also corresponds to sizes measured by DLS (SI table 1 and SI table 2B). High angle annular dark field scanning TEM (HAADF-STEM) was used to

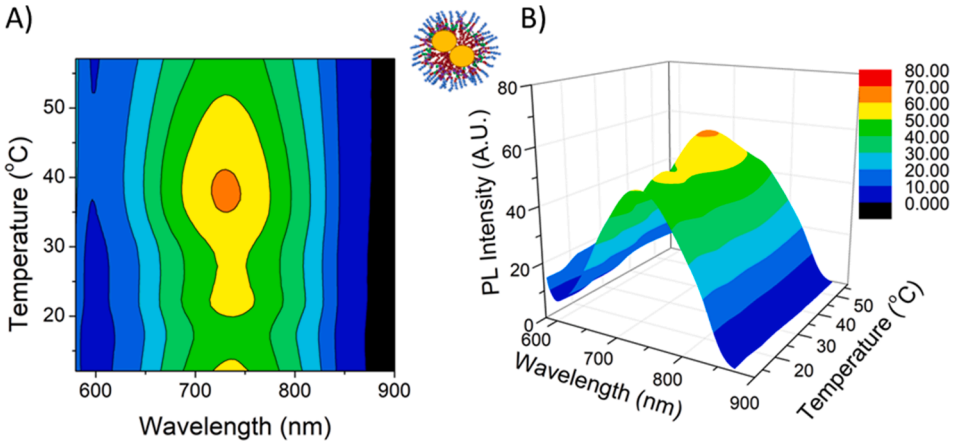

Fig. 2. Photoluminescent properties of gold nanocluster containing micelles. (A) Temperature-dependent heat map and (B) corresponding 3D photoluminescent profile showing enhanced NIR emission at physiological temperature of 37 °C. (λ_{ex} = 550 nm).

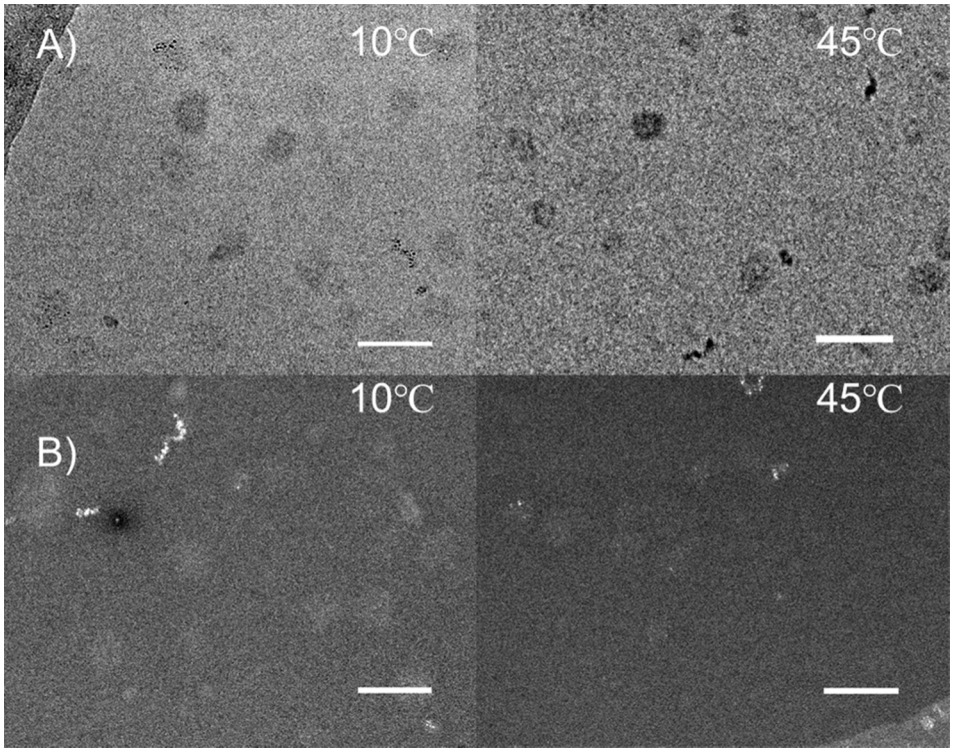

Fig. 3. Morphology of DOX-SH gold nanocluster loaded PNA-PNC micelles. A) Brightfield transmission electron microscopy (TEM) images and B) high-angle annular dark field scanning transmission electron microscopy (HAADF-STEM) images at 10 °C and 45 °C. Scale bars: 100 nm.

complement the bright field TEM images, highlighting all gold structures present within the micellar system, seen as bright white spots (Fig. 3B). Finally EDS measurements confirmed the identity of gold within the micelles (SI fig. 6). In conclusion, the data obtained show the presence of AuNCs located within the core of the core-crosslinked micelles, the density of which increases at elevated temperature.

Internalization studies were performed on MDA-MB-231 cells to investigate the accumulation of DOX-SH containing AuNC-micelles (Fig. 4). In the cells treated with the DOX-containing AuNC micelle formulation, the native fluorescent signal of DOX-SH accumulates inside the treated cells' cytosolic region after 24 h. Free DOX typically accumulates inside the nucleus, which is essential for cytotoxic activity from DNA intercalation to be exerted. [7] This absence of DOX signal inside the nucleus (SI fig. 11) supports the hypothesis that DOX-SH remains bound within the micelles after being internalized for 24 h. The light triggered cytotoxic capacity of the DOX-SH loaded gold nanocluster micelles was investigated on MDA-MB-231 after 24 h incubation with the micelles. Upon NIR light treatment (650 nm, 17 $W.cm^{-2}$), cell death was observed in cells treated with the DOX-SH gold nanocluster micelle formulation localized within the laser spot (Fig. 5). In contrast, cells incubated with AuNC micelles without DOX-SH did not elicit any cell death, demonstrating the need for both AuNCs and DOX-SH. Synergistic action between DOX-SH and local photothermal events caused by the AuNCs may be contributing to enhanced cumulant cytotoxic effects as has also been described in other systems. [6,7] However, no bulk solution temperature changes could be determined, likely due to highly localized heating effects.[39] The herein observed cytotoxicity results also indicate the anticipated release of bound DOX-SH from the cytosolic region to result in its action within the nucleus. Furthermore, the DOX-SH containing AuNC micelle formulation showed no cytotoxicity without irradiation during additional 24 h cell viability assays (SI fig. 9B). Although AuNCs in this size range have previously been reported to be cytotoxic,[40] the cytocompatibility of the system is explained by the AuNCs being bound to the micelles and therefore are unable to enter the nucleus.[41] Taken together, the NIR induced cytotoxicity, delayed cell death hallmarked for DOX and lack of bulk heating strongly suggest that DOX release (due to local intraparticle photothermal effects) is the mechanism responsible for laser induced cytotoxicity.

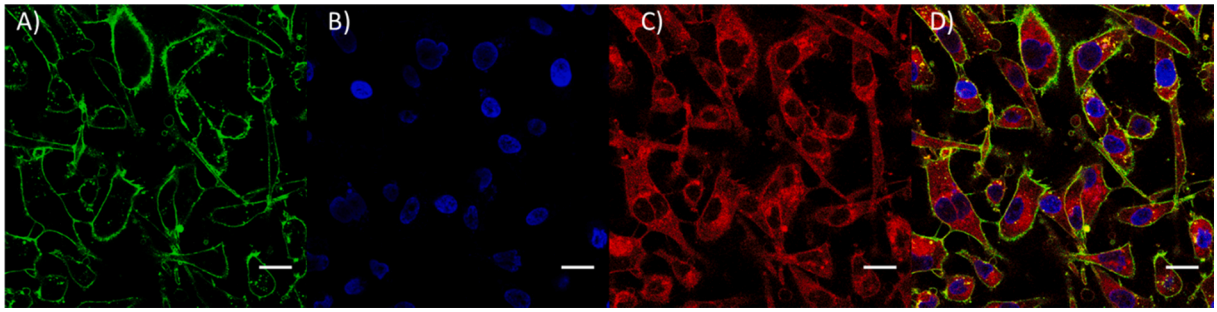

Fig. 4. Laser confocal scanning microscopy images of MDA-MB-231 cells incubated for 24 h with DOX-SH loaded gold nanocluster micelles. Cells are stained for A) cell membranes (oregon green labelled wheat germ agglutinin (WGA), green), B) nucleus (Hoechst 33342, blue. C) DOX-SH is localized by its native fluorescence emission at 595 nm (red). D) Overlay of the three channels. Scale bars: 20 μm.

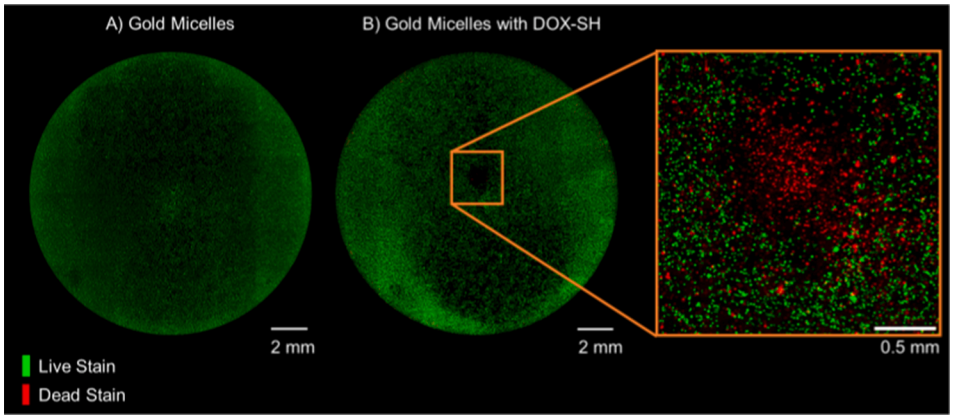

Fig. 5. Representative LIVE/DEAD microscopy images of MDA-MB-231 cells treated for 24 h with gold nanocluster micelles A) containing or B) without DOX-SH and irradiated for 60 min (650 nm, 17 W.cm^{-2}). Cells were stained 24 h after laser irradiation.

Although NIR light is capable of penetrating deeper into tissue than lower optical wavelengths, the application of light triggered systems such as the one we describe here is limited to superficial tumors.[42] For deeper reaching tumor treatments, the use of optic fibers cannulas as a tool to provide high energy local light exposure has been described as a potential solution, and further development of laser technologies will pave the way for deep tumor therapy.[43,44]

4. Conclusions

The herein described results highlight the potential of exploiting thiol-based loading of cytotoxic compounds with AuNCs for laser triggered cell killing. Furthermore, by encapsulating these entities within a core-crosslinked micellar formulation, the physiological stability of such systems can be greatly enhanced allowing cellular internalization without premature drug release.

CRediT authorship contribution statement

Erik R. Hebels: Investigation, Writing - original draft, Visualization, Conceptualization. **Marzieh Najafi:** Resources. **Joep van den Dikkenberg:** Investigation. **Nataliia Beztsinna:** Investigation. **Sanne van de Looij:** Validation. **Danny Wilbie:** Validation. **Johannes Meeldijk:** Investigation. **Mathew Hembury:** Conceptualization, Supervision, Writing - review & editing. **Tina Vermonden:** Conceptualization, Supervision, Writing - review & editing, Funding acquisition.

Declaration of Competing Interest

The authors declare that they have no known competing financial interests or personal relationships that could have appeared to influence the work reported in this paper.

Acknowledgments

The Netherlands Organization for Scientific Research (NWO/Aspasia 015.009.038, NWO/VIDI 13457 and NWO/Industrial Doctorates NWA. ID.17.030 is acknowledged for funding. We thank Prof. W.E. Hennink for scientific discussions. We thank J.A.W. Jong for comments on the manuscript.

Data Availability: The raw/processed data required to reproduce these findings cannot be shared at this time due to technical or time limitations.

Appendix A. Supplementary data

Supplementary data to this article can be found online at https://doi.org/10.1016/j.eurpolymj.2021.110467.

References

[1] M.-C. Daniel, D. Astruc, Gold nanoparticles: assembly, supramolecular chemistry, quantum-size-related properties, and applications toward biology, catalysis, and nanotechnology, Chem. Rev. 104 (2004) 293–346, https://doi.org/10.1021/cr030698+.
[2] M. Hembury, N. Beztsinna, H. Asadi, J.B. van den Dikkenberg, J.D. Meeldijk, W. E. Hennink, T. Vermonden, Luminescent Gold Nanocluster-Decorated Polymeric Hybrid Particles with Assembly-Induced Emission, Biomacromolecules. 19 (7) (2018) 2841–2848, https://doi.org/10.1021/acs.biomac.8b00414.
[3] E. Boisselier, D. Astruc, Gold nanoparticles in nanomedicine: Preparations, imaging, diagnostics, therapies and toxicity, Chem. Soc. Rev. 38 (2009) 1759–1782, https://doi.org/10.1039/b806051g.
[4] M. Mathiyazhakan, C. Wiraja, C. Xu, A Concise Review of Gold Nanoparticles-Based Photo-Responsive Liposomes for Controlled Drug Delivery, Nano-Micro Lett. 10 (2018) 10, https://doi.org/10.1007/s40820-017-0166-0.
[5] E.C. Dreaden, L.A. Austin, M.A. Mackey, M.A. El-Sayed, Size matters: gold nanoparticles in targeted cancer drug delivery, Ther. Deliv. 3 (4) (2012) 457–478, https://doi.org/10.4155/tde.12.21.
[6] T.S. Hauck, T.L. Jennings, T. Yatsenko, J.C. Kumaradas, W.C.W. Chan, Enhancing the Toxicity of Cancer Chemotherapeutics with Gold Nanorod Hyperthermia, Adv. Mater. 20 (20) (2008) 3832–3838, https://doi.org/10.1002/adma.200800921.
[7] F. Yan, W. Duan, Y. Li, H. Wu, Y. Zhou, M. Pan, H. Liu, X. Liu, H. Zheng, NIR-Laser-Controlled Drug Release from DOX/IR-780-Loaded Temperature-Sensitive-Liposomes for Chemo-Photothermal Synergistic Tumor Therapy, Theranostics. 6 (13) (2016) 2337–2351, https://doi.org/10.7150/thno.14937.
[8] R. Mendes, P. Pedrosa, J.C. Lima, A.R. Fernandes, P.V. Baptista, Photothermal enhancement of chemotherapy in breast cancer by visible irradiation of Gold Nanoparticles, Sci. Rep. 7 (2017) 10872, https://doi.org/10.1038/s41598-017-11491-8.
[9] H. Qian, M. Zhu, Z. Wu, R. Jin, Quantum sized gold nanoclusters with atomic precision, Acc. Chem. Res. 45 (9) (2012) 1470–1479, https://doi.org/10.1021/ar200331z.
[10] R. Weissleder, A clearer vision for in vivo imaging, Nat. Biotechnol. 19 (4) (2001) 316–317, https://doi.org/10.1038/86684.
[11] P.K. Jain, X. Huang, I.H. El-Sayed, M.A. El-Sayed, Noble Metals on the Nanoscale: Optical and Photothermal Properties and Some Applications in Imaging, Sensing, Biology, and Medicine, Acc. Chem. Res. 41 (12) (2008) 1578–1586, https://doi.org/10.1021/ar7002804.
[12] G. Yang, J. Liu, Y. Wu, L. Feng, Z. Liu, Near-infrared-light responsive nanoscale drug delivery systems for cancer treatment, Coord. Chem. Rev. 320–321 (2016) 100–117, https://doi.org/10.1016/j.ccr.2016.04.004.
[13] Y. Zhong, C. Wang, L. Cheng, F. Meng, Z. Zhong, Z. Liu, Gold Nanorod-Cored Biodegradable Micelles as a Robust and Remotely Controllable Doxorubicin Release System for Potent Inhibition of Drug-Sensitive and -Resistant Cancer Cells, Biomacromolecules. 14 (7) (2013) 2411–2419, https://doi.org/10.1021/bm400530d.
[14] B. He, H.-Y. Hu, T. Tan, H. Wang, K.-X. Sun, Y.-P. Li, Z.-W. Zhang, IR-780-loaded polymeric micelles enhance the efficacy of photothermal therapy in treating breast cancer lymphatic metastasis in mice, Acta Pharmacol. Sin. 39 (1) (2018) 132–139, https://doi.org/10.1038/aps.2017.109.
[15] M. Talelli, M. Iman, A.K. Varkouhi, C.J.F. Rijcken, R.M. Schiffelers, T. Etrych, K. Ulbrich, C.F. van Nostrum, T. Lammers, G. Storm, W.E. Hennink, Core-crosslinked polymeric micelles with controlled release of covalently entrapped doxorubicin, Biomaterials. 31 (30) (2010) 7797–7804, https://doi.org/10.1016/j.biomaterials.2010.07.005.
[16] M. Talelli, M. Barz, C.J.F. Rijcken, F. Kiessling, W.E. Hennink, T. Lammers, Core-crosslinked polymeric micelles: Principles, preparation, biomedical applications

and clinical translation, Nano Today. 10 (1) (2015) 93–117, https://doi.org/10.1016/j.nantod.2015.01.005.
[17] C.J. Rijcken, C.J. Snel, R.M. Schiffelers, C.F. van Nostrum, W.E. Hennink, Hydrolysable core-crosslinked thermosensitive polymeric micelles: Synthesis, characterisation and in vivo studies, Biomaterials. 28 (36) (2007) 5581–5593, https://doi.org/10.1016/j.biomaterials.2007.08.047.
[18] Q. Zhang, M. Yang, Y.e. Zhu, C. Mao, Metallic Nanoclusters for Cancer Imaging and Therapy, Curr. Med. Chem. 25 (12) (2018) 1379–1396, https://doi.org/10.2174/0929867324666170331122757.
[19] T. Chen, S. Xu, T. Zhao, L. Zhu, D. Wei, Y. Li, H. Zhang, C. Zhao, Gold Nanocluster-Conjugated Amphiphilic Block Copolymer for Tumor-Targeted Drug Delivery, ACS Appl. Mater. Interfaces. 4 (11) (2012) 5766–5774, https://doi.org/10.1021/am301223n.
[20] F. Zhou, B. Feng, H. Yu, D. Wang, T. Wang, J. Liu, Q. Meng, S. Wang, P. Zhang, Z. Zhang, Y. Li, Cisplatin Prodrug-Conjugated Gold Nanocluster for Fluorescence Imaging and Targeted Therapy of the Breast Cancer, Theranostics. 6 (5) (2016) 679–687, https://doi.org/10.7150/thno.14556.
[21] H. Chen, B. Li, X. Ren, S. Li, Y. Ma, S. Cui, Y. Gu, Multifunctional near-infrared-emitting nano-conjugates based on gold clusters for tumor imaging and therapy, Biomaterials. 33 (33) (2012) 8461–8476, https://doi.org/10.1016/j.biomaterials.2012.08.034.
[22] R. Vankayala, C.-L. Kuo, K. Nuthalapati, C.-S. Chiang, K.C. Hwang, Nucleus-Targeting Gold Nanoclusters for Simultaneous In Vivo Fluorescence Imaging, Gene Delivery, and NIR-Light Activated Photodynamic Therapy, Adv. Funct. Mater. 25 (37) (2015) 5934–5945, https://doi.org/10.1002/adfm.201502650.
[23] X.-R. Song, N. Goswami, H.-H. Yang, J. Xie, Functionalization of metal nanoclusters for biomedical applications, Analyst. 141 (11) (2016) 3126–3140, https://doi.org/10.1039/C6AN00773B.
[24] M. Hembury, C. Chiappini, S. Bertazzo, T.L. Kalber, G.L. Drisko, O. Ogunlade, S. Walker-Samuel, K.S. Krishna, C. Jumeaux, P. Beard, C.S.S.R. Kumar, A.E. Porter, M.F. Lythgoe, C. Boissière, C. Sanchez, M.M. Stevens, Gold–silica quantum rattles for multimodal imaging and therapy, Proc. Natl. Acad. Sci. 112 (7) (2015) 1959–1964, https://doi.org/10.1073/pnas.1419622112.
[25] M. Najafi, E. Hebels, W.E. Hennink, T. Vermonden, Poly(N -isopropylacrylamide): Physicochemical Properties and Biomedical Applications, in: Temp. Polym., John Wiley & Sons Ltd, Chichester, UK, 2018: pp. 1–34. https://doi.org/10.1002/9781119157830.ch1.
[26] K.W.M. Boere, J. van den Dikkenberg, Y. Gao, J. Visser, W.E. Hennink, T. Vermonden, Thermogelling and chemoselectively cross-linked hydrogels with controlled mechanical properties and degradation behavior, Biomacromolecules. 16 (9) (2015) 2840–2851, https://doi.org/10.1021/acs.biomac.5b00802.
[27] K.W.M. Boere, B.G. Soliman, D.T.S. Rijkers, W.E. Hennink, T. Vermonden, Thermoresponsive Injectable Hydrogels Cross-Linked by Native Chemical Ligation, Macromolecules. 47 (7) (2014) 2430–2438, https://doi.org/10.1021/ma5000927.
[28] A.F.S.A. Habeeb, Determination of free amino groups in proteins by trinitrobenzenesulfonic acid, Anal. Biochem. 14 (3) (1966) 328–336, https://doi.org/10.1016/0003-2697(66)90275-2.
[29] H. Cabral, K. Kataoka, Progress of drug-loaded polymeric micelles into clinical studies, J. Control. Release. 190 (2014) 465–476, https://doi.org/10.1016/j.jconrel.2014.06.042.
[30] M. Grabolle, M. Spieles, V. Lesnyak, N. Gaponik, A. Eychmüller, U. Resch-Genger, Determination of the Fluorescence Quantum Yield of Quantum Dots: Suitable Procedures and Achievable Uncertainties, Anal. Chem. 81 (15) (2009) 6285–6294, https://doi.org/10.1021/ac900308v.
[31] M. Najafi, N. Kordalivand, M.-A. Moradi, J. van den Dikkenberg, R. Fokkink, H. Friedrich, N.A.J.M. Sommerdijk, M. Hembury, T. Vermonden, Native Chemical Ligation for Cross-Linking of Flower-Like Micelles, Biomacromolecules. 19 (9) (2018) 3766–3775, https://doi.org/10.1021/acs.biomac.8b00908.
[32] M. Kuhlmann, O. Reimann, C.P.R. Hackenberger, J. Groll, Cysteine-Functional Polymers via Thiol-ene Conjugation, Macromol. Rapid Commun. 36 (5) (2015) 472–476, https://doi.org/10.1002/marc.201400703.
[33] F. Aldeek, M.A.H. Muhammed, G. Palui, N. Zhan, H. Mattoussi, Growth of Highly Fluorescent Polyethylene Glycol- and Zwitterion-Functionalized Gold Nanoclusters, ACS Nano. 7 (3) (2013) 2509–2521, https://doi.org/10.1021/nn305856t.
[34] R. Jin, Atomically precise metal nanoclusters: stable sizes and optical properties, Nanoscale. 7 (5) (2015) 1549–1565, https://doi.org/10.1039/C4NR05794E.
[35] N. Goswami, Q. Yao, Z. Luo, J. Li, T. Chen, J. Xie, Luminescent Metal Nanoclusters with Aggregation-Induced Emission, J. Phys. Chem. Lett. 7 (6) (2016) 962–975, https://doi.org/10.1021/acs.jpclett.5b02765.
[36] Z. Liu, Y. Huang, X. Yi, B. Fu, G. Yuan, J. Wang, J. Li, Y. Zhang, Analysis of Photoluminescence Thermal Quenching: Guidance for the Design of Highly Effective p-type Doping of Nitrides, Sci. Rep. 6 (2016) 32033, https://doi.org/10.1038/srep32033.
[37] M. Borzenkov, G. Chirico, L. D'Alfonso, L. Sironi, M. Collini, E. Cabrini, G. Dacarro, C. Milanese, P. Pallavicini, A. Taglietti, C. Bernhard, F. Denat, Thermal and Chemical Stability of Thiol Bonding on Gold Nanostars, Langmuir. 31 (29) (2015) 8081–8091, https://doi.org/10.1021/acs.langmuir.5b01473.
[38] M. Denel-Bobrowska, A. Marczak, Structural modifications in the sugar moiety as a key to improving the anticancer effectiveness of doxorubicin, Life Sci. 178 (2017) 1–8, https://doi.org/10.1016/j.lfs.2017.04.009.
[39] C.P. Kabb, R.N. Carmean, B.S. Sumerlin, Probing the surface-localized hyperthermia of gold nanoparticles in a microwave field using polymeric thermometers, Chem. Sci. 6 (10) (2015) 5662–5669, https://doi.org/10.1039/C5SC01535A.
[40] Y.u. Pan, S. Neuss, A. Leifert, M. Fischler, F. Wen, U. Simon, G. Schmid, W. Brandau, W. Jahnen-Dechent, Size-Dependent Cytotoxicity of Gold Nanoparticles, Small. 3 (11) (2007) 1941–1949, https://doi.org/10.1002/smll.200700378.
[41] A. Al Zaki, J.Z. Hui, E. Higbee, A. Tsourkas, Biodistribution, Clearance, and Toxicology of Polymeric Micelles Loaded with 0.9 or 5 nm Gold Nanoparticles, J. Biomed. Nanotechnol. 11 (2015) 1836–1846, https://doi.org/10.1166/jbn.2015.2142.
[42] S. Stolik, J.A. Delgado, A. Pérez, L. Anasagasti, Measurement of the penetration depths of red and near infrared light in human "ex vivo" tissues, J. Photochem. Photobiol. B Biol. 57 (2-3) (2000) 90–93, https://doi.org/10.1016/S1011-1344(00)00082-8.
[43] Ji Hee Kang, Young Tag Ko, Dual-selective photodynamic therapy with a mitochondria-targeted photosensitizer and fiber optic cannula for malignant brain tumors, Biomater. Sci. 7 (7) (2019) 2812–2825, https://doi.org/10.1039/C9BM00403C.
[44] Tadanobu Nagaya, Shuhei Okuyama, Fusa Ogata, Yasuhiro Maruoka, Peter L. Choyke, Hisataka Kobayashi, Endoscopic near infrared photoimmunotherapy using a fiber optic diffuser for peritoneal dissemination of gastric cancer, Cancer Sci. 109 (6) (2018) 1902–1908, https://doi.org/10.1111/cas.13621.